External front instabilities induced by a shocked particle ring

V. Rodriguez,* R. Saurel, G. Jourdan, and L. Houas
Aix–Marseille Université, CNRS, IUSTI UMR 7343, 13013 Marseille, France
(Received 19 February 2014; revised manuscript received 28 August 2014; published 21 October 2014)

The dispersion of a cylindrical particle ring by a blast or shock wave induces the formation of coherent structures which take the form of particle jets. A blast wave, issuing from the discharge of a planar shock wave at the exit of a conventional shock tube, is generated in the center of a granular medium ring initially confined inside a Hele-Shaw cell. With the present experimental setup, under impulsive acceleration, a solid particle-jet formation is observed in a quasi-two-dimensional configuration. The aim of the present investigation is to observe in detail the formation of very thin perturbations created around the external surface of the dispersed particle layer. By means of fast flow visualization with an appropriate recording window, we focus solely on the first instants during which the external particle ring becomes unstable. We find that the critical area of the destabilization of the external ring surface is constant regardless of the acceleration of the initial layer. Moreover, we observe in detail the external front perturbation wavelength, rendered dimensionless by the initial ring perimeter, and follow its evolution with the initial particle layer acceleration. We report this quantity to be constant regardless of the evolution of the initial particle layer acceleration. Finally, we can reasonably assert that external front perturbations depend solely on the material of the particles.

DOI: 10.1103/PhysRevE.90.043013 PACS number(s): 47.40.Nm, 45.70.−n

I. INTRODUCTION

A. State of the art

Solid-particle dispersion (and even dispersion of liquids and hybrid mixtures of liquids and solid particles) induced by an explosive event has often been observed. This mechanism appears in the nature, such as by volcanic eruptions or during the impact of a solid projectile in a granular medium, as reported by Kedrinskiy [1] and Lohse *et al.* [2], respectively. In applied aspects, during the last decade [3–7], the formation of solid-particle jets has been studied intensively in three-dimensional spherical configurations by the use of explosives. Certain trends have been made apparent in these studies. First, the dispersion of the particle layer depends on the ratio between the weight of the particles and that of the explosive [3]. There exists a minimum layer velocity for the observation of jets, which depends on the latter ratio. Below this velocity, there are no particle jets. Furthermore, the formation of such jetting behavior seems to start very early in the process. Finally, for spherical configurations, particle layer fragmentation begins at the same volume in different experiments [7]. A more focused study was carried out recently by Frost *et al.* [8]. In this article dispersion was performed by means of explosives in a cylindrical configuration in order to reduce three-dimensional effects. The solid particles were saturated with liquid. Results show that wet particles produce more jets than dry ones. Similar behavior appears with liquids. The dispersion of water without particles produces many more jets of liquid drops than solid particles or mixtures of solid particles and liquid [9]. Some results connected with these previous works are reported in the present paper.

In addition to experimental studies, some numerical works have been conducted in parallel in order to support the experiments. Thus, Xu *et al.* (2013) performed a numerical study concerning solid-particle dispersion at the mesoscopic scale and for a cylindrical shock tube configuration [10]. The results reveal that the mechanism of particle jetting can be induced by two parameters: the driver gas jets induced by the shock wave through the initial particle layer in the inner surface of the ring and inelastic collisions between particles.

In spite of these various research studies, aimed at understanding the physical mechanism which governs such jetting instabilities, the selection mechanism is still not understood. Furthermore, the three-dimensional nature of these configurations increases the difficulty of analyzing the experimental results. The aim of our quasi-two-dimensional configuration is to conduct reliable repetitive experiments using a ring of particles in radial expansion trapped in a Hele-Shaw cell. We have previously shown that the mechanism of such jetting formation occurs in four steps [11], as illustrated in Fig. 1. This represents a video sequence covering the expansion of a ring of flour (different from experiments previously presented) with a diameter of 10 μm impulsively accelerated by a Mach number 1.39 shock wave: first, the formation of jets inside the particle ring at a very early stage, denoted J_i, as shown in Fig. 1(b); second, the appearance of short-wavelength perturbations at short times, denoted J_e^{st}, as shown in Fig. 1(c); third, the crossing of the J_i jets through the particle layer to form the outside particle jets at long times, denoted J_e^{lt}, as shown in Fig. 1(e); and finally, the coalescence of the J_e^{lt} jets due to transverse motion, which induces a decrease in the number of jets with time. These jets at very long times are denoted J_e^{vlt} as shown in Fig. 1(f).

B. Objectives

The latter study, after describing in detail the experimental setup and protocol, highlighted the presence of various perturbations during the displacement of the granular medium induced by shock and blast waves. We focus the present study on the first instants when the external front of particles becomes rough (the second step described above) in order to detect other elements never observed before. The reason for this is that,

*vincent.rodriguez@univ-amu.fr

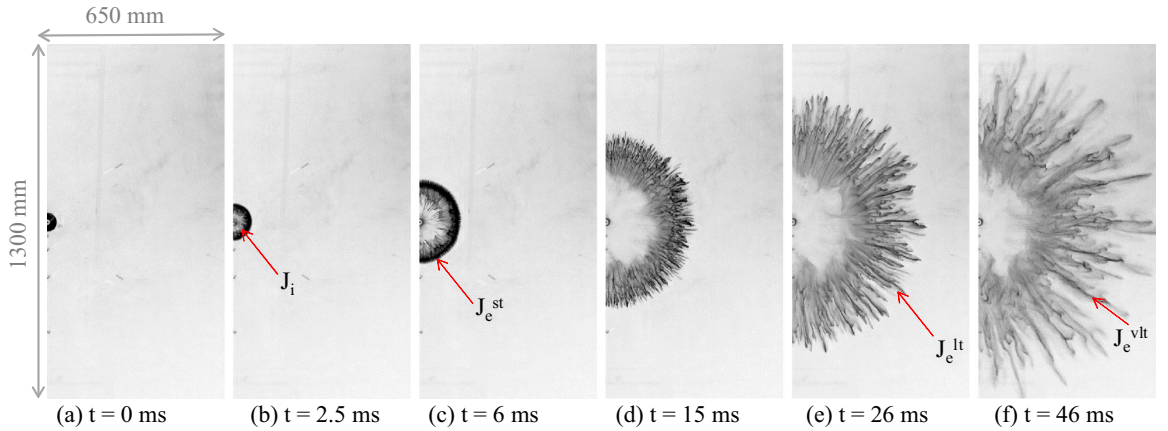

FIG. 1. (Color online) Sequence of events occuring during typical solid-particle jet formation under shock-wave acceleration. The Mach number of the incident shock wave is 1.39. The particle material is flour, the density of which is 1530 kg/m^3 and the mean particle diameter 10 μm. The initial external and internal diameters of the ring are 60 and 20 mm, respectively. J_i are the internal jets, J_e^{st} are the short-wavelength external perturbations at short times, J_e^{lt} are the external jets at long times resulting from the internal jets which have crossed the front of particles, and J_e^{vlt} are the external jets at very long times.

since the selection appears very rapidly inside the ring, we are convinced of the importance that we have to focus our attention on the first instants to understand the selection mechanism. In order to record the whole phenomenon, in our previous study, we used a large window of visualization (1300 × 1300 mm^2). It was therefore almost impossible to obtain precise details concerning the second step of the mechanism. The objectives of the present work are to change the visualization field and to focus solely on the instants during which the external front of particles becomes rough. The purpose is to study this step in detail, i.e., to determine the distance at which the phenomenon occurs and the wavelength of such perturbations. Many other experiments were conducted under different conditions (particle material, initial acceleration, and initial ring diameter), the results of which are presented below.

This article is organized as follows. In Sec. II, we present the experimental setup and the refinement of visualization. In Sec. III, we report the new results, namely, the experimental observations made from the closeup view of the external front. In Sec. IV, we summarize the results obtained in the present study.

II. EXPERIMENTAL SETUP

Experiments are carried out using a small conventional shock tube which produces moderate overpressure. The shock tube creates a blast wave at its exit, i.e., an impulsive pressure jump followed by a rapid decrease in pressure, which propagates radially into the Hele-Shaw cell. A diagram of the experimental setup is presented in Fig. 2. The small conventional shock tube (T32) has a diameter of 32 mm. It is fitted vertically beneath a Hele-Shaw cell inside which the dispersion of particles takes place as shown in Fig. 2. The incident shock wave is directed towards the center of the ring, inducing the dispersion of the particle layer. The particle jet formation is recorded by a Photron Fastcam SA1 high-speed camera and the breaking mode of the granular layer subjected to an impulsive overpressure is studied. In this experimental campaign, three materials were used—flour (the finest corn flour), talc, and polystyrene spheres—the properties of which are listed in Table I. We measured the size of the particles with a particle size analyzer. We checked results in the literature for flour [12,13] and talc [14]. The initial rings of particles were 40, 60, and 90 mm in diameter, respectively. The Mach number of the incident shock wave propagating within the shock tube ranged from 1.1 to 1.45, and the corresponding impulsive peak of overpressure from 0.7 to 4 bars. We changed the frame acquisition frequency from 4000 to 20 000 fps, with a spatial resolution of 512 × 512 pixels, and the size of the observation window from 1300 × 1300 to 100 × 100 mm^2. With this refinement, we were able to record in detail the transition of the external particle front from a smooth to a

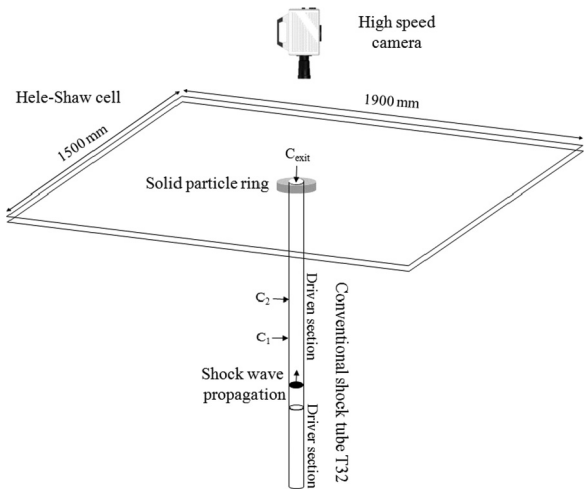

FIG. 2. Sketch of the experimental setup. The C_1 and C_2 pressure gauges allow the determination of the incident shock-wave Mach number. The C_{exit} pressure gauge records the pressure history at the center of the particle ring. The driver section of the shock tube is 210 mm long and its driven section is 945 mm long. The space between the two plates is 4 mm and the initial rings of particles are 40, 60, and 90 mm in diameter.

TABLE I. Particle properties, where ρ_p and Φ_p are the material density (in kg/m^3) and the particle diameter (in μm), respectively.

Particles	ρ_p	Φ_p
Flour	1530	14.5 ± 5
Polystyrene spheres	1050	10 ± 2
Talc	2700	10.5 ± 2.5

rough state and try to better understand the physical behavior of particle jetting.

III. RESULTS

A. Experimental observations

Figure 3 shows a sequence of recorded photographs covering the first instants of particle-jet formation. This example was obtained with a flour particle ring 60 mm in diameter and impulsively accelerated by a shock wave with a Mach number of 1.21. In this example, the transition of the external particle front from a smooth to a rough state is highlighted. At $t = 0$ [Fig. 3(a)] the incident shock wave interacts with the internal surface of the particle ring. From $t = 0$ to about $t = 3.25$ ms, the particle ring moves radially and its external front stays smooth while internal jets J_i are formed. For these specific experimental conditions, the transition time for the passage from a smooth to a rough state is about $t = 3.25$ ms [Fig. 3(d)]. This time increases with the decrease in the particle layer acceleration and with the increase in the initial diameter of the ring. It corresponds to the emergence of the external perturbations at short times J_e^{st} (the rough state). With these new detailed observations, it appears that this time seems to be correlated with the beginning of the crossing of the internal jet J_i through the particle front. From $t = 3.25$ ms to $t = 4.75$ ms, the J_e^{st} continue to grow and at $t = 4.75$ ms we clearly observe a quasiuniform distribution of these very small perturbations. Their wavelength is considerably shorter than that of the internal particle jets J_i. In the present case, we estimated the wavelength to be equal to 3.3 mm, which corresponds to a total of 190 perturbations.

B. "Critical" diameter and area

In several experiments we measured the distance from the origin (external diameter) at which the external particle front becomes unstable. We defined this diameter as the "critical" diameter, denoted Φ_c. It should be noted that the initial ring diameter is defined by Φ_0. Results are plotted in Fig. 4, where experimental points are grouped for flour, talc, and polystyrene spheres and three initial ring diameters (40, 60, and 90 mm). On the basis of these results, we observe that the "critical" diameter Φ_c is constant regardless of the initial acceleration γ for each particle ring size and each material. The initial particle ring acceleration is deduced from the experimentally reconstructed trajectories between 0 and 3.5 ms. Φ_c increases

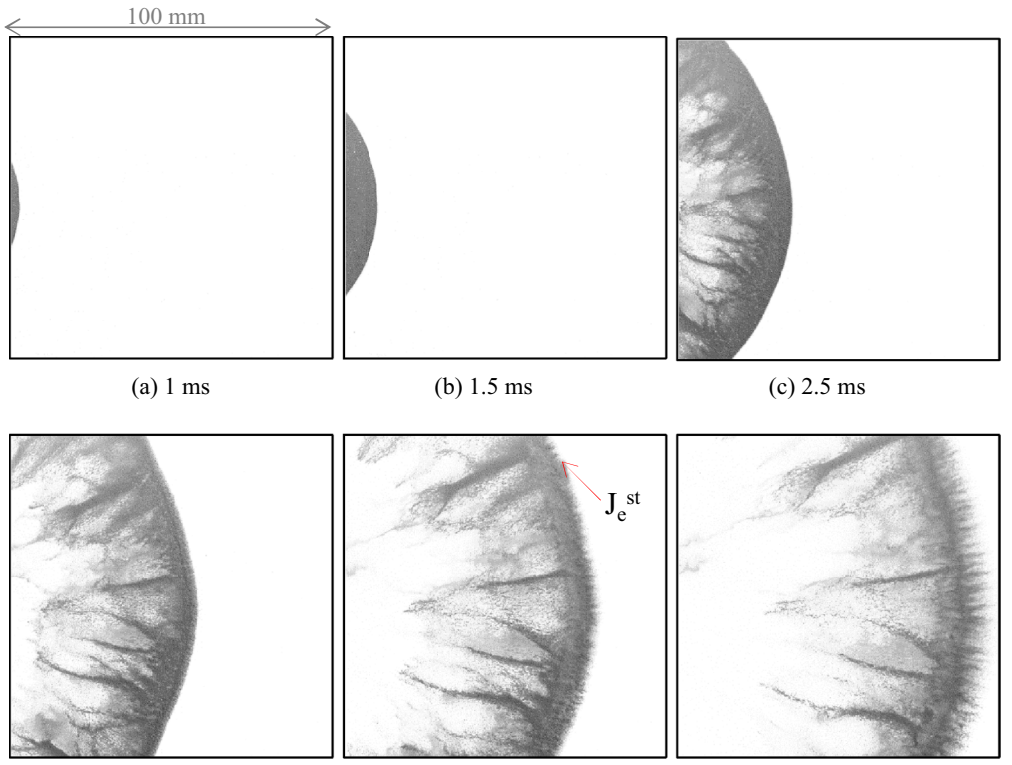

(a) 1 ms (b) 1.5 ms (c) 2.5 ms

(d) 3.25 ms (e) 4 ms (f) 4.75 ms

FIG. 3. (Color online) Closeup visualization, in reversed colors, of the first instants of the solid particle dispersion by a shock wave with Mach number 1.21 (run T32 No 131), corresponding to an initial overpressure peak of 2.9 bar. The particle material is flour, the density of which is 1530kg/m^3 and the mean particle diameter 10 μm. The initial external and internal diameters of the ring are 60 and 20 mm, respectively. J_e^{st} are the short-wavelength external perturbations at short times.

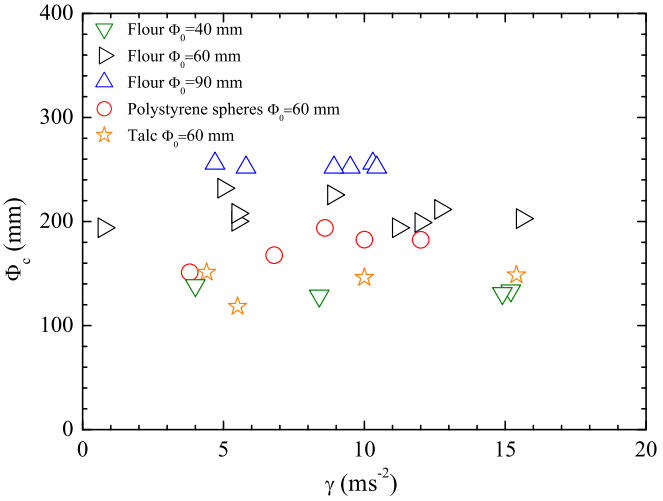

FIG. 4. (Color online) "Critical" diameter Φ_c, at which the external particle front becomes unstable, with different initial ring sizes (diameters of 40, 60, and 90 mm) versus the initial particle layer acceleration γ between $t = 0$ and $t = 3.5$ ms. The size of the symbol represents the error bar.

logically with the initial ring diameter but it is surprising that it seems to evolve totally at random with the density of the material. This observation suggests that other parameters, such as cohesion, equivalent surface tension, and collisions between particles (polystyrene particles are perfectly spherical, whereas talc and flour are angular), influence the formation of these perturbations. Moreover, in Fig. 5 we have plotted the area covered by the particles at the instant when the external front becomes unstable, denoted A_c, rendered dimensionless by the initial particle ring area, denoted $A_0 = (\pi \Phi_0^2)/4$, versus the initial particle ring acceleration γ. It should be note that the critical area A_c is not equal to $(\pi \Phi_c^2)/4$ because the particles

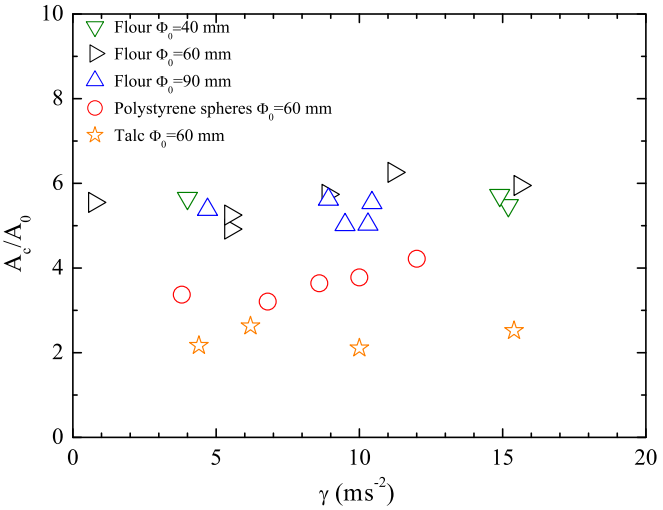

FIG. 5. (Color online) "Critical" area A_c, at which the external particle front becomes unstable, covered by particles dimensionless by the initial particle ring area A_0 versus the initial particle layer acceleration γ between $t = 0$ and $t = 3.5$ ms. The size of the symbol represents the error bar.

do not cover the whole disk delimited by the external particle front. This critical area A_c is measured with image processing software in which the frames are binarized in black and white pixels. Particles are represented by black pixels and the software extracts the surface covered by these (in square pixels). Square pixels are converted to square millimeters. As the critical diameter Φ_c, this critical area A_c is constant for a given initial ring diameter and material regardless of the initial particle ring acceleration. However, with the dimensionless quantity "A_c/A_0" it was possible to merge all the experimental points, for each material, resulting from different initial particle ring diameters. Consequently, the critical diameter Φ_c and the critical area A_c are constant regardless of the initial layer acceleration but evolve with the initial diameter of the particle ring. For a given initial diameter of the ring (60 mm, for example, in our study), they are also different for each particle material. As the particle layer becomes unstable with the same covered surface and under given initial experimental conditions specific for each particle material, we can speculate that an "equivalent" surface tension for this heterogeneous gas-particle mixture can be defined as fluid surface tension, which can include cohesion between particles. It may include parameters intrinsic to the particle layer such as cohesion and interactions between particles. Similar jetting behavior appears with water. In such a configuration, the number of jets is much higher than in a solid-particle configuration, as shown by Frost *et al.* [9]. A second series of experiments, with dry and wet particles saturated with liquid, was performed [8,9]. The following conclusions may be drawn: there are more jets with wet particles saturated with liquid than dry particles. Moreover, an analogy can be drawn between the phenomenon of liquid drop fragmentation and the jetting behavior of solid particles. In the work by Villermaux and Bossa on drop fragmentation on impact [15], such jetting behavior is observed with jets of liquid droplets. In addition, their experimental geometry is almost similar to ours (pseudo-two-dimensional). Thus, the hypothesis that there is an equivalent surface tension for the heterogeneous gas-particle (dry or wet) mixture can be put forward.

C. Evolution of the external front perturbation wavelength

With these new recording settings, it was now possible to accurately estimate the number of short-time external front perturbations J_e^{st}. We carried out additional experiments using new closeup recording settings. These new experiments were only conducted with flour particles and just with a change in the external ring diameter to focus on the J_e^{st} wavelength (all other parameters need to be fixed). The wavelength λ_p of these perturbations can be ascertained from the figures. It is determined when the ring of particles reaches the critical diameter Φ_c. This is because these small jets begin to appear at this distance. We plot, in Fig. 6, the experimental points corresponding to the J_e^{st} wavelength, rendered dimensionless by the initial ring perimeter $\pi \Phi_0$, versus the initial ring acceleration γ with different initial ring diameters. Results clearly show that the J_e^{st} perturbation wavelength around the external front of the ring is independent of the initial acceleration, which is different from that of the main particle jets as shown in [11] (first, J_i inside and, then, $J_e^{\mathrm{lt/vlt}}$ outside the ring). Indeed, we

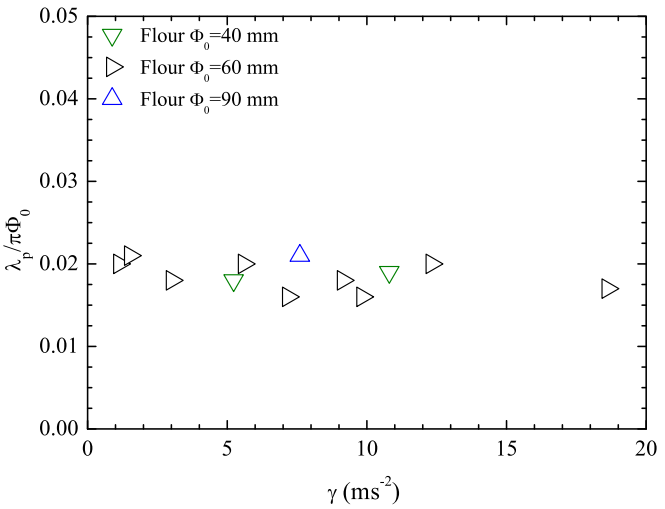

FIG. 6. (Color online) External front perturbation wavelength λ_p dimensionless by the initial ring perimeter $\pi\,\Phi_0$ versus the initial ring acceleration. The size of the symbol represents the error bar.

observed previously that the selection of the main particle jets depends on the initial ring acceleration γ. The results presented in Fig. 6, coupled with the previous ones concerning particle jets, lead us to believe that there is, on the one hand, formation of main particle jets (first, J_i inside and, then, $J_e^{\mathrm{lt/vlt}}$ outside the ring) which continue to grow throughout the duration and whose wavelength depends on the initial layer acceleration. On the other hand, there are smaller perturbations (J_e^{st} all around the external front) which remain constant and are absorbed by the main particle jets at long times. In view of these results, we can reasonably assert that the external front perturbations depend solely on the particle material. Moreover, this point reinforces the idea that these perturbations arise from the effect of an equivalent surface tension, including cohesion between particles, for this mixture which breaks up the particle layer of the external front into very thin clusters.

IV. CONCLUSION

We have presented a quasi-two-dimensional experimental study focused on the first instants of particle-jet formation associated with the dispersion of an impulsive accelerated granular material. Several particle ring sizes and materials were studied. Only the formation of external front perturbations at short times J_e^{st} was considered. The closeup visualization enabled us to see in detail the transition of the external particle front from a smooth to a rough state. This transition takes place at the same covered surface by the ring in expansion, regardless of the initial acceleration. The results lead us to believe that another parameter is involved in the destabilization of an impulsively dispersed layer of particles. This parameter would seem to be intrinsic to the particle layer, such as cohesion and interactions between particles. Finally, we highlighted the fact that the formation of small external perturbations at short times is independent of the main jet formation at long times and depends solely on the particle material. This smaller perturbation formation is absorbed by the main jet formation at long times and its wavelength is independent of the initial layer acceleration.

[1] V. Kedrinskiy, Shock Waves **18**, 451 (2009).
[2] D. Lohse, R. Bergmann, R. Mikkelsen, C. Zeilstra, D. van der Meer, M. Versluis, K. van der Weele, M. van der Hoef, and H. Kuipers, Phys. Rev. Lett. **93**, 198003 (2004).
[3] D. L. Frost, S. Goroshin, and F. Zhang, in *Proceedings of the 21st Military Aspects of Blast and Shock* (ORTRA, Jerusalem, Israel, 2010), p. 36; http://www.mabs.ch/spiezbase/mabs21/Abstracts%20CORRECT%20with%20Page%20No_S35.pdf.
[4] F. Zhang, D. L. Frost, P. A. Thibault, and S. B. Murray, Shock Waves **10**, 431 (2001).
[5] D. L. Frost, C. Ornthanalai, Z. Zarei, V. Tanguay, and F. Zhang, J. Appl. Phys. **101**, 113529 (2007).
[6] A. M. Milne, C. Parrish, and I. Worland, Shock Waves **20**, 41 (2010).
[7] C. Parrish and I. Worland in *Proceedings of the 28th International Symposium on Shock Waves*, edited by K. Kontis (Springer, Manchester, UK, 2011), Vol. 2, p. 107.
[8] D. L. Frost, Y. Grégoire, O. Petel, S. Goroshin, and F. Zhang, Phys. Fluids **24**, 091109 (2012).
[9] D. L. Frost, J. F. Ruel, Z. Zarei, S. Goroshin, Y. Grégoire, F. Zhang, A. M. Milne, and A. Longbottom, in *Proceedings of the 22nd Military Aspects of Blast and Shock* (Bourges, France, 2012).
[10] T. Xu, F.-S. Lien, H. Ji, and F. Zhang, Shock Waves **23**, 619 (2013).
[11] V. Rodriguez, R. Saurel, G. Jourdan and L. Houas, Phys. Rev. E **88**, 063011 (2013).
[12] B. Sullivan, W. E. Engebretson and M. L. Anderson, Cereal Chem. **37**, 436 (1960).
[13] R. R. Irani and W. S. Fong, Cereal Chem. **38**, 67 (1961).
[14] J. Ferrer, J. F. Montes, M. A. Vilarino, CHEST **122**, 1018 (2002).
[15] E. Villermaux and B. Bossa, J. Fluid Mech. **668**, 412 (2011).